Unsupervised Learning for Detection of Defects in Pulsed Infrared Thermography of Metals

Xin Zhang and Jafar Saniie
ECASP Research Laboratory (http://ecasp.ece.iit.edu)
Department of Electrical and Computer Engineering
Illinois Institute of Technology, Chicago, IL, U.S.A.

Sasan Bakhtiari and Alexander Heifetz
Nuclear Science and Engineering Division
Argonne National Laboratory
Lemont, IL, U.S.A.

2022 IEEE International Conference on Electro Information Technology (eIT) | 978-1-6654-8009-3/22/$31.00 ©2022 IEEE | DOI: 10.1109/eIT53891.2022.9814026

***Abstract*— Metal Additive Manufacturing (AM) is a promising method for cost-efficient fabrication of complex shape structures for applications in harsh environment, such as in a nuclear reactor. However, internal defects (pores) occur in high-strength AM alloys, which are manufactured with Laser Powder Bed Fusion (LPBF) AM method. Pulsed Infrared Thermography (PIT) is an efficient nondestructive evaluation (NDE) method to examine actual structures, because this method offers one-sided non-contact measurements, and fast processing of large sample areas. However, imaging of material defects, particularly defects with sizes at microscopic level, is challenging. In this paper, we benchmark the performance of several Unsupervised Learning (UL) algorithms designed to enhance imaging of microscopic defects in metals with PIT. UL aims to learn the latent principal patterns (dictionaries) in PIT data to detect defects with minimal human supervision. Performance of Independent Component Analysis (ICA), Sparse Coding (SC), Principal Component Analysis (PCA) and Exploratory Factor Analysis (EFA) was compared using F-score, UL model training time and defects reconstruction time. We obtained the average F-score of 0.75, and a highest F-score of 0.89 for the EFA algorithm. Overall, EFA outperforms other UL algorithms considered in this study.**

Keywords —Unsupervised Learning, Metallic Microscopic Defects Detection, Pulsed Infrared Thermography, Metal Additively Manufacturing

I. INTRODUCTION

Additive Manufacturing (AM) is an emerging method for the fabrication of complex shape custom structures. AM of high strength alloys, which are used in nuclear energy applications, is currently based on the Laser Powder Bed Fusion (LPBF) method [1]. Because of inherent features, the LPBF method introduces material defects, such as keyhole and lack of fusion microscopic pores, which can potentially become a seed for a crack. Therefore, nondestructive evaluation (NDE) is needed to verify the integrity of AM structures before they enter service, followed by a periodic in-service inspection.

There exist several approaches for NDE of metallic structures. In general, ultrasonic testing is the common method for NDE of metals flaws. This method is scalable to arbitrary structure sizes and surface shapes [2]. However, ultrasonic testing requires direct contact of an ultrasonic probe with material surface and involves time-consuming raster scanning to create images. The Eddy Current (EC) imaging has been commonly used for in-service NDE in nuclear reactor applications because this method uses the non-contact inductive probes resilient to harsh environments. However, EC measurements can be affected by material surface shape and temperature irregularities [3]. The X-ray Computed Tomography (XCT) can inspect metals with high imaging resolution but requires structures with symmetric body of revolution shapes [4]. Because AM metallic structures usually involve complex patterns without symmetry, XCT faces challenges in imaging internal defects in actual AM structures.

Pulsed Infrared Thermography (PIT) offers several advantages for post-manufacturing NDE of AM structures because this method is non-contact, one-sided, and scalable to arbitrary structure size [5]. The PIT method involves rapid deposition of a heat pulse on the material surface, followed by the recording of time-resolved sequential measurements of surface temperature distribution using a fast frame Infrared (IR) camera. As heat deposited on the material surface starts diffusing into the bulk, the internal defects behave as thermal resistances. This slows down surface temperature decay in regions above the defects. Information about the internal defects can be extracted by analyzing the time-dependent stack of thermography images.

Detection of material defects in thermography images is affected by edge blurring due to diffusion-based imaging, IR camera noise, and uneven heating of the specimen with thermal pulse [6]. General signal processing methods, such as Gaussian, Median filtering and Savitzky–Golay filtering can enhance defects detection but are not adapted to specific requirements of problems in thermal imaging [7]. A more specialized thermographic signal reconstruction (TSR) method [8], applies curve fitting algorithm to enhance the accuracy of detection. However, this method requires analyzing a large number of thermography frames, which is time-consuming. Recently, a data-processing method has been introduced and uses fewer polynomial fitting coefficients than TSR by employing the Gauss-Newton algorithm [9]. However, this reduced detection accuracy. In addition, sixteen matrices with temperature information need to be stored, which increases the complexity to implementation. In our previous research, we have developed the Neural Learning based Blind Source Separation (NLBSS) algorithm [10] and the thermal tomography 3D imaging

978-1-6654-8009-3/22/$31.00 ©2022 IEEE

algorithm [11] [12] to detect internal defects in AM metals with sizes larger than 1 mm located at various depths. However, imaging microscopic defects in metals requires analyzing weak thermal signatures comparable in amplitude to IR camera noise level.

In this paper, we investigate performance of UL algorithms in detection of subsurface microscopic level defects in metals. UL aims to learn the latent principal patterns in data with minimal human supervision [13]. In PIT, the UL is trained to learn the principal thermal signatures in thermography data, and remove the redundant information. These learned thermal patterns are used for reconstruction to enhance defects detection. In this study, several state-of-art UL algorithms, including the independent component analysis (ICA) [14], sparse coding (SC) [15], principle component analysis (PCA) [16], and exploratory factor analysis (EFA) [17] were compared using the F-score, training time and run time. By using UL, we demonstrate imaging metallic defects of various sizes and depths in high-strength alloys.

II. Pulsed Infrared Thermography System

Figure 1 shows the schematic of Pulsed Infrared Thermography (PIT) system. As shown in Figure 1, the PIT experimental setup includes the IR camera, high energy electrical capacitor, pulse trigger, flash lamp and PC. In PIT, the pulse trigger initializes a high-energy capacitor discharge through a while light flash lamp to rapidly heat the specimen surface. A fast frame IR camera is synchronized to record images of material surface temperature transients. The stack of observed thermography images is acquired and further processed using the UL algorithms to enhance the detection of material defects in images.

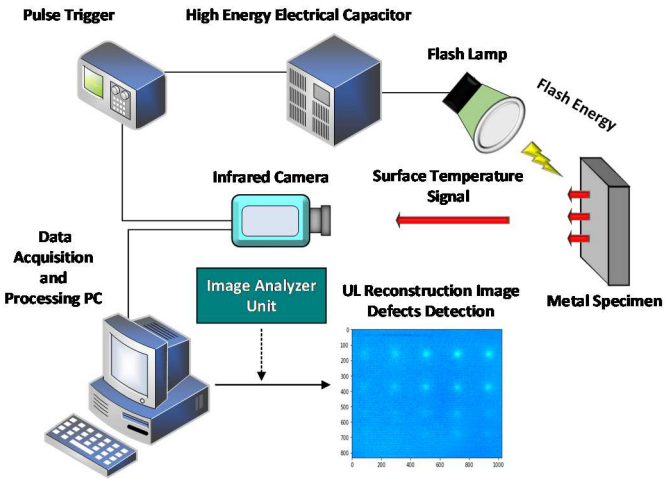

Figure 1. Pulsed Infrared Thermography System Setup

the high-speed mid-wave IR camera (FLIR x8501sc) is used to record high-resolution thermography images with the noise equivalent temperature difference (NETD) of 20mK. The Balcar ASYM 6400 electrical capacitor is used to deliver a pulse of 6.4 kJ/2ms thermal energy through the flash lamp to heat the specimen surface. As heat deposited on the material surface starts diffusing into the specimen, the internal defects act as thermal resistance which slows down the surface temperature decay.

In this study, the focus is on imaging defects in stainless steel 316L (SS316L), which is the primary material for passive structures in high-temperature fluid liquid metal and molten salt-cooled advanced reactors. In previous studies, we have demonstrated the capability of PIT in imaging calibrated defects with sizes on the order of 1mm-diameter in SS316L [6]. These calibrated defects consisted of imprinted hemispherical regions containing un-sintered powder in AM SS316 specimens, and flat bottom hole (FBH) indentations drilled in SS316 specimens. In this study, we investigate performance of UL in processing PIT images to detect microscopic FBH defects in SS316 specimens.

III. Unsupervised Learning for Imaging Defects in Metals

ICA, PCA, SC and EFA UL algorithms were developed for analysis of PIT images. Performance of UL algorithms was compared using F-score, training time, and testing time. The calculations were carried out on the Intel (R) Core (TM) i7-8750H, CPU@2.20GHz 2.21GHz computer with NVIDIA GTX 1070 GPU.

A. Independent Component Analysis (ICA)

The ICA method is used to separate the multivariate mixed signals into the corresponding cluster of independent subcomponents. In PIT, thermography frames consist of a stack of time-dependent mixed temperature signals, which follow Gaussian distribution. This is because the distribution of the sum of N temperature measurements approaches Gaussian distribution as $N \rightarrow \infty$, regardless of the distribution of each temperature measurement [14]. These temperature signals can be clustered into independent subcomponents by maximizing the non-Gaussian distribution of training data, while ensuring that the subcomponents are uncorrelated. The subcomponents correspond to material surface regions of defects and non-defects and are used for image reconstruction to enhance visualization of defects. In training the ICA, the fast fixed-point optimization algorithm [14] is applied to search for the direction to maximize the non-Gaussian to estimate the independent subcomponents.

B. Principal Component Analysis (PCA)

The PCA method aims to find in data the low dimensional latent patterns, which are called principal components (PC). This is implemented by maximizing the data variance and minimizing the Mean Squared Error (MSE) between the original data and reconstructed data. The PC's are orthogonal to each other. The largest data variance is contained in the first PC, and each subsequent PC provides decreasing contribution to the total data variance. In processing PIT images, the PCA is trained to find the latent principal patterns in thermography data. These principal thermal patterns are used for image reconstruction to enhance visualization of defects in the specimen. In training the PCA, the Lagrange multiplier method [18] is applied to iteratively search for the principal thermal patterns to minimize the MSE.

C. Sparse Coding (SC)

The SC method is used to find the sparse representation in data by searching for the optimized basis vectors during training. Compared with ICA and PCA, the SC is more flexible to train the latent base vectors because these vectors are not required to be orthogonal. In processing PIT images, the SC is trained to find the sparse thermal patterns by minimizing the reconstruction loss between the original data and reconstructed data. The sparse thermal patterns are used for image reconstruction to visualize defects in the specimen. In training the SC, the matching pursuit algorithm [19] is applied to iteratively search for the sparse thermal patterns to minimize the reconstruction loss.

D. Exploratory Factor Analysis (EFA)

The EFA method aims to find the linear transformation of the low dimensional latent factors in data by reducing redundant information and random noises. The EFA is advantageous to model data variance independently in each direction of the input space, which adds flexibility in training the latent factors. In addition, the EFA model can perform better in the presence of heteroscedastic noise. In processing of PIT images, the EFA is trained to find the latent factors in thermography data. The maximum likelihood estimation [14] is used as the objective function, and the Expectation-Maximization (EM) [20] method is applied to iteratively search for the optimal thermal factors to maximize the objective function. The EM iteration alternates between conducting the expectation (E) step and the maximization (M) step. In the E-step, a lower bound function is created to calculate the expectation of the log-likelihood using the current estimate for the parameters. In the M-step, the parameters are updated by maximizing the expectation of log-likelihood found in the E-step. These optimal thermal factors are used for reconstruction to enhance visualization of defects in the specimen.

E. Accuracy Measurement for Detection of Defects

In this study, the F-score is used as the metric of accuracy of defects detection. This metric is an indicator how well the UL algorithm can separate the true signals from noise. The F-score is proportional to the number of defects from the total set of calibrated defects in the specimen that are detected. The value of F-score is in the range from 0 to 1, with the higher value indicating better performance. The F-score is calculated as:

$$F_{score} = \frac{(\beta+1)\times(Precision\times Recall)}{\beta^2\times(Precision+Recall)} \quad (1)$$

$$Precision = T_p/(T_p + F_p) \quad (2)$$

$$Recall = T_p/(T_p + F_n) \quad (3)$$

In equations above, T_p = true positive, F_p = false positive, F_n = false negative. *Precision* is the ratio of true positive to the sum of true and false positives. *Recall* parameter is the fraction of true positives to the sum of true positives and false negatives. β is the tradeoff parameter, which determines whether *Precision* or *Recall* is more important. In this study, we set β = 1, which indicates that *Precision* and *Recall* are equally important.

F. Experimental Results for Detection of Defects

To evaluate performance of UL algorithms in processing of PIT images (thermograms), we recorded images of SS316L FBH metallic plate with calibrated internal defects of various sizes and depths. Figure 2(a) shows the photograph of the front surface of the specimen plate with EDM (Electron Discharge Machining)-drilled microscopic FBH. Figure 2(b) shows the photograph of the back surface of the specimen plate for PIT imaging with Krylon ultra flat black spray paint. The specimen plate is 3 mm thick. The FBH defects varied from 200µm to 500µm in diameter, with depths below the specimen surface ranging from 100µm to 500µm.

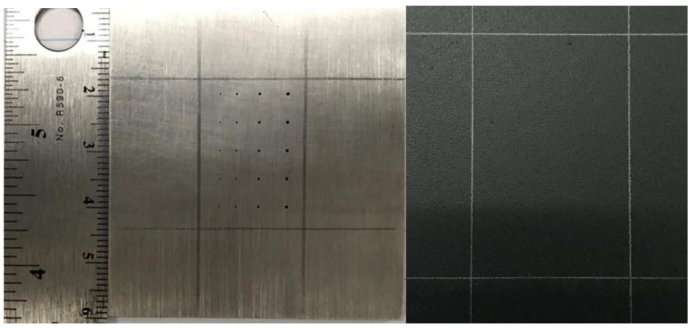

a b

Figure 2. Front Surface (a), and Back Surface (b) of SS316L FBH Specimen Plate

The design drawing of the FBH defects introduced into the SS316L specimen is shown in Figure 3(a). The drawing with labels indicates diameters and depths of the FBH defects. The design pattern of the defects is a grid with diameters ϕ = 0.5 mm, 0.4 mm, 0.3 mm and 0.2 mm, and depths d = 0.1 mm, 0.2 mm, 0.3 mm, 0.4 mm and 0.5 mm. Distance between nearest FBH centers along the horizontal direction is 5 mm. Distances between canters of nearest FBH centers along vertical dimensions are 3 mm, 4 mm and 5 mm. The diameters of defects decrease along the vertical direction from top to bottom. Defect depths increase along the horizontal direction from the right to left. The red wireframe box with dashed line shows the target imaging area, which includes 20 FBH defects with various diameters and depths. The SS316L FBH specimen plate was imaged with the PIT system using the IR camera settings of 237Hz frame rate and 832 x 1024 pixels. Figure 3(b) shows one recorded thermogram. A total of 1180 thermograms were acquired during a total imaging time of approximately 5 seconds. The UL algorithms were trained with recorded thermograms for the enhanced reconstruction of material defects in the images.

Figures 3(c) to 3(f) show images reconstructed with ICA, SC, PCA and EFA algorithms, respectively. While defects cannot be seen in the raw thermography image in Figure 3(b), all panels corresponding to results of four UL algorithms show material defects in images. Quantitatively, reconstruction with the EFA algorithm in Figure 3(f) shows more material defects, as compared to images obtained with other UL algorithms in this study.

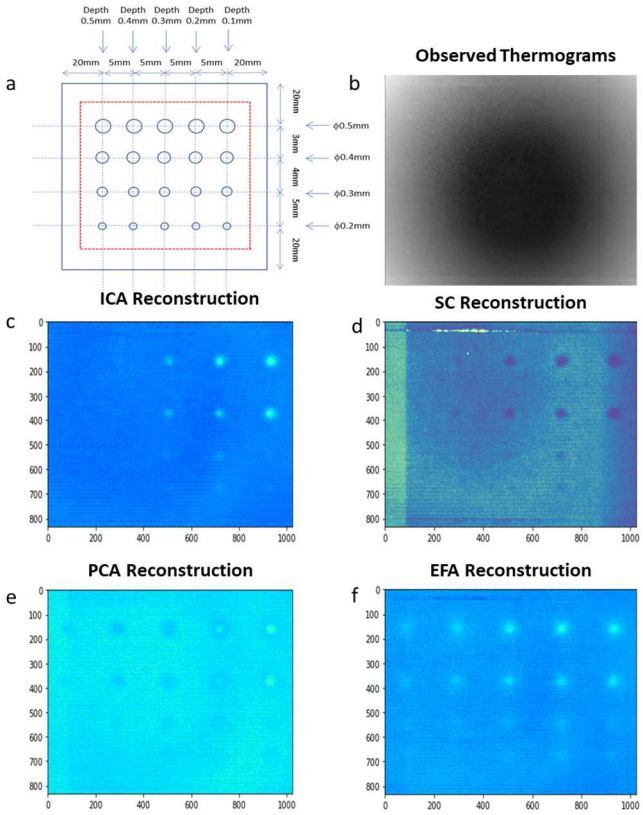

Figure 3. UL processing of thermography data. (a) Map of FBH defects in SS316 specimen; (b) Example of recorded raw thermogram; (c) ICA reconstruction; (d) SC reconstruction; (e) PCA reconstruction; (f) EFA reconstruction.

Table 1 shows quantitative benchmarking of the UL algorithms, where the performance metrics are the F-score, UL model training time and defects reconstruction time. For the benchmarking study, we trained UL models with 30 latent dictionaries.

TABLE 1. UL PERFORMANCE COMPARISON FOR METAL DEFECTS DETECTION

Model	F-score	Model Training Time (Second)	Defects Reconstruction Time (Second)
PCA	0.67	81.90	45.67
EFA	0.89	338.86	21.72
ICA	0.67	382.71	23.31
SC	0.75	330.75	43.23

The F-score values are distributed between 0.67 and 0.89, with the average value across all algorithms of 0.75. This indicates a reasonably good accuracy of performance for all algorithms. PCA and ICA algorithms yield the same accuracy of defects detection judging by the F-score. The SC algorithm outperforms the PCA and ICA in terms of the F-score, while the EFA achieves the highest F-score of all algorithms. PCA requires substantially less time (by approximately a factor of 4) to train the model, as compared to SC, EFA and ICA algorithms. ICA and EFA are approximately twice as fast in the reconstruction of defects as PCA and SC algorithms. Because EFA achieves the highest F-score and the shortest time for reconstruction of defects, we conclude that EFA outperforms other algorithms considered in this study.

IV. Conclusion

Metal AM is a promising method for the cost-efficient fabrication of high-strength complex-shape structures. However, AM process can leave residual internal defects (pores) in AM structures, which need to be detected nondestructively. PIT offers a number of advantages in NDE of metals, including one-sided non-contact measurements and fast processing of large sample areas. In this paper, we proposed several UL algorithms to enhance visualization of microscopic defects in PIT images metals. UL aims to learn the principal latent patterns in thermography data to detect defects with minimal human supervision. Our study benchmarked performance ICA, SC, PCA and EFA algorithms, which were compared using F-score, UL model training time and testing (defects reconstruction) time. UL algorithms were trained with thermograms obtained with PIT imaging of calibrated microscopic FBH defects introduced into the SS316 plate. We obtained the average F-score of 0.75 across all UL algorithms, and the highest F-score of 0.89 for the EFA algorithm. Overall, EFA outperforms other algorithms considered in this study. Future work is to explore neural networks, such as the auto-encoder, and other machine learning algorithms to improve the performance of defects detection.

V. Acknowledgment

This work was supported in part by the US Department of Energy, Office of Nuclear Energy, Nuclear Energy Enabling Technology (NEET) Advanced Methods of Manufacturing (AMM) program, under contract DE-AC02-06CH11357.

References

[1] S. A. Khairallah, A. T. Anderson, A. Rubenchik, and W. E. King, ‘‘Laser powder-bed fusion additive manufacturing: Physics of complex melt flow and formation mechanisms of pores, spatter, and denudation zones,’’ *Acta Mater.*, vol. 108, pp. 36–45, Apr. 2016.

[2] X. Zhang, X. R. Yu and J. Saniie, ‘‘Intelligent Ultrasonic Systems for Material Texture Recognition using Data-Efficient Neural Networks,’’ in *Proc. IEEE Int. Ultrason. Symp. (IUS)*, Xi’an, China, Sep. 2021.

[3] W. Du, Q. Bai, Y. Wang, and B. Zhang, ‘‘Eddy current detection of subsurface defects for additive/subtractive hybrid manufacturing,’’ *Int. J. Adv. Manuf. Technol.*, vol. 95, nos. 9–12, pp. 3185–3195, Apr. 2018.

[4] A. Du Plessis, S. G. Le Roux, G. Booysen, and J. Els, ‘‘Quality control of a laser additive manufactured medical implant by X-ray tomography,’’ *3D Printing Additive Manuf.*, vol. 3, no. 3, pp. 175–182, Sep. 2016.

[5] X. Zhang, J. Saniie, S. Bakhtiari and A. Heifetz, ‘‘Compression of Pulsed Infrared Thermography Data With Unsupervised Learning for Nondestructive Evaluation of Additively Manufactured Metals,’’ *IEEE Access*, vol. 8, pp. 175054–175062, 2020.

[6] X. Zhang, J. Saniie, W. Cleary, and A. Heifetz, ‘‘Quality control of additively manufactured metallic structures with machine learning of thermography images,’’ *JOM*, vol. 72, no. 12, pp. 4682–4694, Oct. 2020.

[7] X. Zhang, J. Saniie, and A. Heifetz, ‘‘Spatial Temporal Denoised Thermal Source Separation in Images of Compact Pulsed Thermography System for Qualification of Additively Manufactured Metals,’’ in *Proc. IEEE Int.*

Conf. Electro. Inf. Technol. (EIT), Mt. Pleasant, MI, USA, May 2021.

[8] D. L. Balageas, J.-M. Roche, F.-H. Leroy, W.-M. Liu, and A. M. Gorbach, ''The thermographic signal reconstruction method: A powerful tool for the enhancement of transient thermographic images,'' *Biocyber. Biomed. Eng.*, vol. 35, no. 1, pp. 1–9, 2015.

[9] W. F. Da Silva, R. A. C. Melo, M. Grosso, G. R. Pereira, and D. B. Riffel, ''Active thermography data-processing algorithm for nondestructive testing of materials,'' *IEEE Access*, vol. 8, pp. 175054–175062, 2020.

[10] X. Zhang, J. Saniie, and A. Heifetz, ''Neural learning based blind source separation for detection of material defects in pulsed thermography images,'' in *Proc. IEEE Int. Conf. Electro. Inf. Technol. (EIT)*, Chicago, IL, USA, Sep. 2020.

[11] X. Zhang, J. Saniie and A. Heifetz, ''Detection of defects in additively manufactured stainless steel 316L with compact infrared camera and machine learning algorithms,'' *JOM*, vol. 72, no. 12, pp. 4244–4253, Oct. 2020.

[12] A. Heifetz, D. Shribak, X. Zhang, J. Saniie, Z. L. Fisher, T. Liu, J. G. Sun, T. Elmer, S. Bakhtiari, and W. Cleary, ''Thermal tomography 3D imaging of additively manufactured metallic structures,'' *AIP Adv.*, vol. 10, no. 10, Oct. 2020, Art. no. 105318.

[13] D. Greene, P. Cunningham, and R. Mayer, ''Unsupervised learning and clustering,'' in *Machine Learning Techniques for Multimedia*. Berlin, Germany: Springer, 2008.

[14] A. Hyvärinen, ''The fixed-point algorithm and maximum likelihood estimation for independent component analysis,'' *Neural Process. Lett.*, vol. 10, no. 1, pp. 1–5, 1999.

[15] J. Mairal, F. Bach, J. Ponce, and G. Sapiro, ''Online dictionary learning for sparse coding,'' in *Proc. 26th Annu. Int. Conf. Mach. Learn. (ICML)*, New York, NY, USA, Jun. 2009.

[16] I. T. Jolliffe and J. Cadima, ''Principal component analysis: A review and recent developments,'' *Phil. Trans. Roy. Soc. A, Math., Phys. Eng. Sci*., vol. 374, no. 2065, Apr. 2016, Art. no. 20150202.

[17] M. W. Watkins, ''Exploratory factor analysis: A guide to best practice,'' *J. Black Psychol.*, vol. 44, no. 3, pp. 219–246, Apr. 2018.

[18] D. P. Bertsekas, *Constrained Optimization and Lagrange Multiplier Methods*. Cambridge, MA, USA: Academic, 1982.

[19] X. Zhang, Y. Liu, and X. Wang, ''A sparsity preestimated adaptive matching pursuit algorithm,'' *J. Electr. Comput. Eng.*, vol. 2021, pp. 1–8, Apr. 2021.

[20] A. P. Dempster, N. M. Laird, and D. B. Rubin, ''Maximum likelihood from incomplete data via the EM algorithm,'' *J. Roy. Statist. Soc., B Methodol.*, vol. 39, no. 1, pp. 1–38, 1977.